Journal of Power Sources 233 (2013) 34–42

Contents lists available at SciVerse ScienceDirect

Journal of Power Sources

journal homepage: www.elsevier.com/locate/jpowsour

Effects of current densities on the lithium plating morphology at a lithium phosphorus oxynitride glass electrolyte/copper thin film interface

Fumihiro Sagane [a,b], Ken-ichi Ikeda [a], Kengo Okita [a], Hikaru Sano [b,c], Hikari Sakaebe [b,c], Yasutoshi Iriyama [b,d,*]

[a] Department of Materials Science and Chemical Engineering, Faculty of Engineering, Shizuoka University, 3-5-1 Johoku, Naka-ku, Hamamatsu, Shizuoka 432-8561, Japan
[b] JST, CREST, 5, Sanbancho, Chiyoda-ku, Tokyo 102-0075, Japan
[c] Research Institute for Ubiquitous Energy Devices, National Institute of Advanced Industrial Science and Technology (AIST), 1-8-31 Midorigaoka, Ikeda, Osaka 563-8577, Japan
[d] Department of Materials, Physics and Energy Engineering, Graduate School of Engineering, Nagoya University, Furo-cho, Chikusa-ku, Nagoya 464-8603, Japan

HIGHLIGHTS

- ► Lithium plating morphology at LiPON/Cu thin film is investigated.
- ► The increasing of the current density decreases the size of plated lithium.
- ► The above phenomena are observed by in-situ optical microscopy and SEM.
- ► The electrochemically-plated lithium shows stable and low-resistive reactions.

ARTICLE INFO

Article history:
Received 16 August 2012
Received in revised form
1 December 2012
Accepted 10 January 2013
Available online 7 February 2013

Keywords:
Lithium
Anode
All-solid-state battery
Interface

ABSTRACT

Lithium metal (Li) is electrochemically-grown at the lithium phosphorus oxynitride glass electrolyte (LiPON)/copper (Cu) thin film interface. The plated lithium morphology depends on the current densities, and larger current densities bring about smaller-sized precipitation of Li with larger coverage ratio by the precipitates. Both scanning electron microscopy and *in-situ* optical microscopy observations reveal that the lithium tends to grow at the lithium pre-plated place. Large potential drop was observed at the initial lithium plating process, suggesting that the nucleation process requires large activation energy at the initial lithium plating process at the LiPON/Cu interface. The resultant morphology-controlled *in-situ* prepared Li provides stable and low-resistive Li/LiPON interface compared with the vacuum-evaporated Li thin film.

1. Introduction

Usage of electrode active materials with large capacity is directly-effective expedient to develop advanced rechargeable lithium batteries (LIBs) with high energy density, and lithium metal is an ultimate anode material with the capacity of 3860 mAh g^{-1}, about 10 times larger value than that of graphite anode [1]. However, lithium metal anode has crucial problems to be applied in conventional LIBs using liquid electrolyte because of the dendritic growth of lithium metal during the repetition of charge–discharge reactions, leading to the short circuit of the battery and then the source of serious accidents to the battery. On the other hand, lithium metal anode has been widely used in all-solid-state thin-film lithium batteries (TFBs), where lithium phosphorus oxynitride glass electrolyte ($\sim Li_{3.3}PO_{3.7}N_{0.3}$) is typically used in them [2–6]. In those batteries, lithium metal thin film prepared by vacuum evaporation has been mounted in general, and quite stable charge–discharge reactions (20,000 cycles with 0.001% capacity loss) have been realized.

However, there are still unsolved problems on lithium plating-stripping reactions on inorganic solid electrolytes and one of them is the degradation of the reactions at higher current densities. For example, Neudecker et al. have reported that their TFBs (Li/LiPON/$LiCoO_2$) can repeat stable charge–discharge cycles at 1 mA cm^{-2}, while the capacity was degraded at higher current densities (5 mA cm^{-2}). They have pointed out that less favorable

* Corresponding author. Department of Materials, Physics and Energy Engineering, Graduate School of Engineering, Nagoya University, Furo-cho, Chikusa-ku, Nagoya 464-8603, Japan.
E-mail address: iriyama@numse.nagoya-u.ac.jp (Y. Iriyama).

0378-7753/$ – see front matter © 2013 Elsevier B.V. All rights reserved.
http://dx.doi.org/10.1016/j.jpowsour.2013.01.051

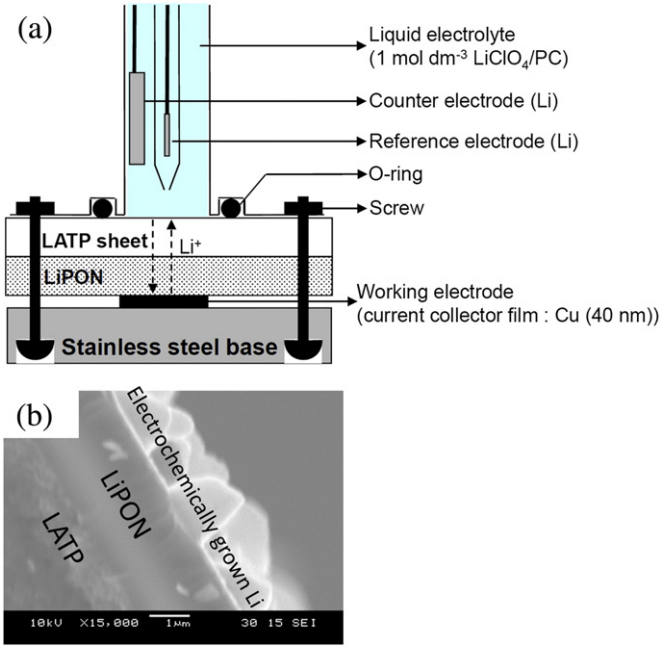

Fig. 1. (a) Schematic image of electrochemical measurement cell for Li plating-stripping reaction. (b) A typical cross-sectional SEM image of LATP sheet/LiPON/Cu cell after Li plating reaction.

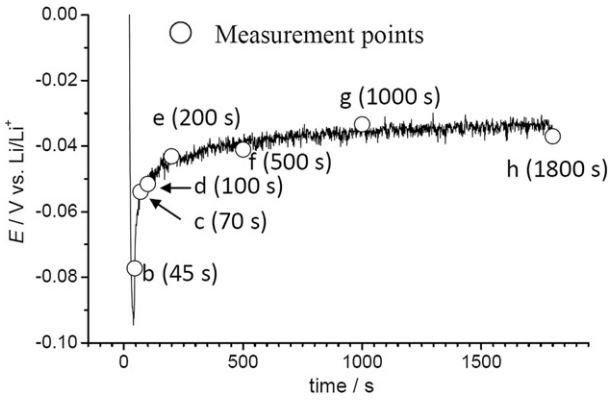

Fig. 3. An initial lithium plating curve of the LATP sheet/LiPON/Cu cell measured in *in-situ* optical microscopy measurement cell shown in Fig. 2. $I = 50\ \mu A\ cm^{-2}$.

morphology of the lithium metal may occur during the repetition of charge–discharge cycles [7]. Fleutot et al. has prepared Li/LiPONB/TiOS (LiPONB:LiPON including a few percentage of boron, TiOS:-TiO_yS_z) thin film battery and found that the battery impedance rapidly increases by the charging at higher current densities. Based on the A.C. impedance analysis, they have concluded that the capacity fading originates from the increasing of the Li/LiPONB interface due to the decreasing of the Li/LiPONB contact area by the morphology change of lithium electrode [8]. These results indicate that morphology change at the lithium/solid electrolyte can be a source of the degradation of TFBs using lithium metal anode [9].

Metal plating-stripping reactions on inorganic solid electrolytes have been examined extensively in silver ion conductive inorganic solid electrolyte system, and various fundamental properties and novel applications of silver plating-stripping reactions have been reported, such as kinetics of electrode reaction [10], interfacial capacity [11], switching device [12], micro writing [13], all-solid-state batteries [14,15], etc. Among them, silver growth morphology and their controls have been studied by various authors [16–19]. Corish and O'Briain [16], and Ohachi and Taniguchi [17] have developed a technique to control silver whisker growth formation using

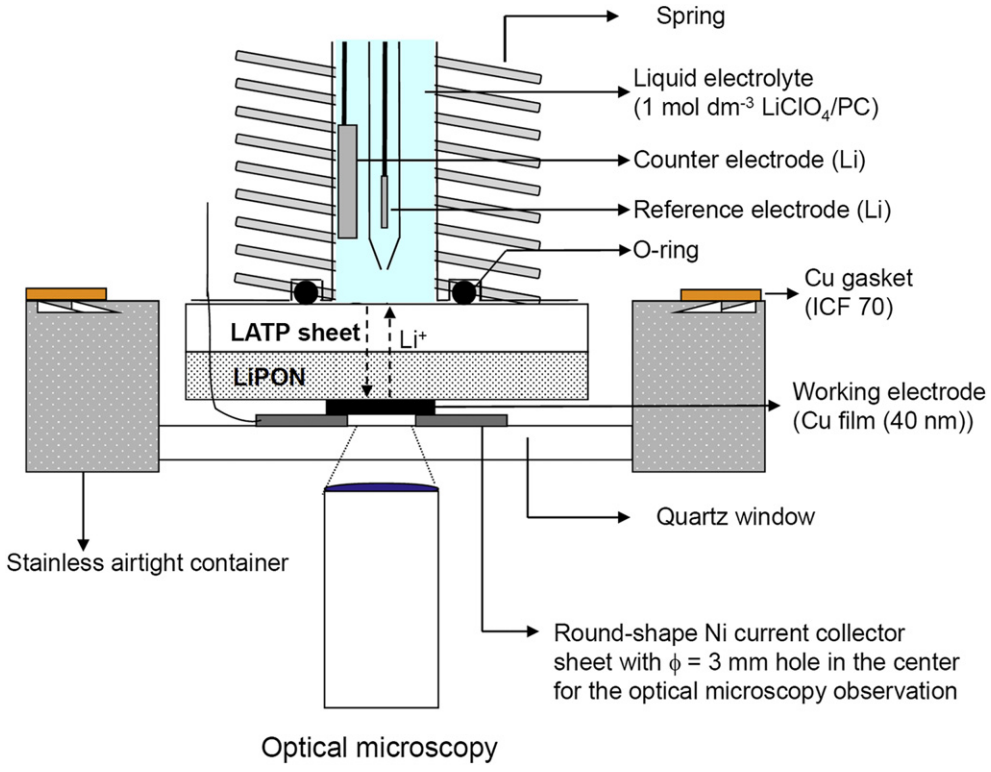

Fig. 2. Schematic image of *in-situ* optical microscopy measurement cell of Li plating reaction to the LATP sheet/LiPON/Cu cell.

galvanic cell and have discussed the growth mechanism. Peppler and Janek have investigated the cathodic deposition of silver on silver bromide single crystal using micro electrode and reported that dendritic growth of silver is observed at higher current densities, while whisker growth at smaller ones [19]. Although there are many works on the morphology control and growth mechanism in case of the silver system, there are few studies on the lithium plating-stripping reaction on inorganic solid electrolytes though the morphology can influence on the battery performances of all-solid-state rechargeable lithium batteries (SSBs) using lithium metal anode [9].

A purpose of this paper is to investigate the effect of current densities on the lithium plating morphology at the LiPON/Cu interface. The lithium plating reactions were carried out at the LiPON/Cu interface, where LiPON film was deposited on mirror-polished solid electrolyte sheet ($Li_{1+x+y}Al_yTi_{2-y}Si_xP_{3-x}O_{12}$ (LATP sheet), Ohara Inc., Kanagawa, Japan [20]). By using flat LATP sheet without any volume change during the lithium plating-stripping

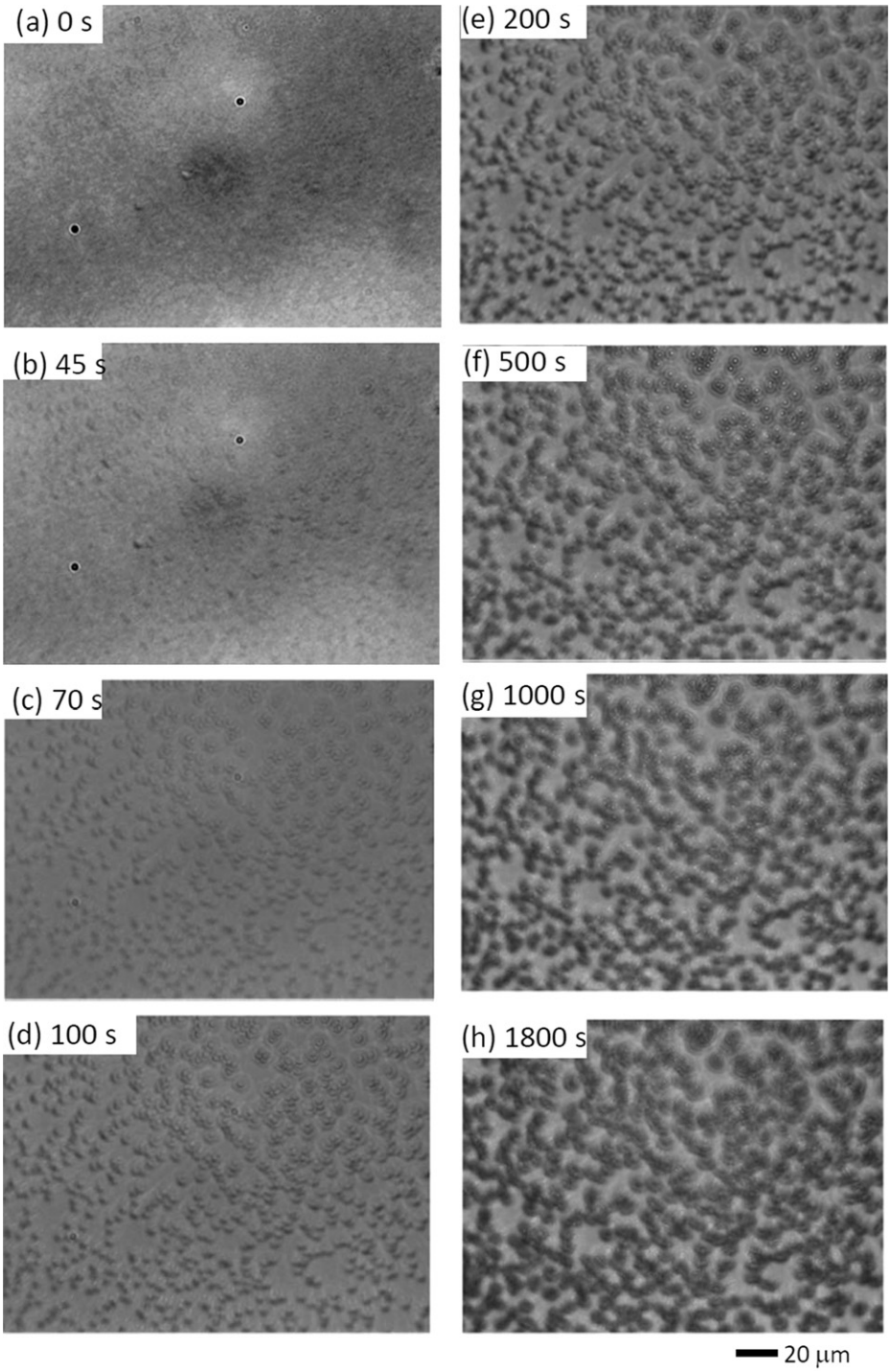

Fig. 4. *In-situ* optical microscopy images during Li plating process of the LATP sheet/LiPON/Cu cell. Those images were captured at (a) 0 s (pristine), (b) 45 s, (c) 70 s, (d) 100 s, (e) 200 s, (f) 500 s, (g) 1000 s, and (h) 1800 s. The measurement points are denoted as circles in Fig. 3.

process, non-uniform reactivity due to thickness distribution of LiPON, substrate convexity, and degradation of lithium supplying material (thin-film positive electrode materials in case of the TFBs) will be removed, which must be helpful to simplify the Li plating-stripping phenomena. We will show that the plated lithium morphology depends on the current densities and that the lithium is preferentially plated to the pre-plated region. Also, we found that the resultant morphology-controlled lithium formed on LiPON is effective to stabilize lithium plating-stripping reactions at higher current densities as compared with the vacuum-evaporated lithium.

2. Experimental

Thin films of LiPON (2.5 μm in thickness) were deposited on one side of mirror-polished LATP sheet by RF magnetron sputtering. The sputtering was carried out following the conditions reported by Bates et al. [2,3]. Copper thin film (40 nm in thickness, 0.20 cm^2 in area) was deposited on the LiPON film by pulsed laser deposition, and LATP/LiPON/Cu multi-layered solid electrolyte sheets (Cu-cell) were prepared. Also, lithium metal film (5 μm in thickness) was deposited on the LiPON film by vacuum evaporation incorporated in argon-filled grove box (dew point: −90 °C) in place of the Cu film, and LATP/LiPON/Li cell (V-Li-cell) was fabricated.

Lithium plating-stripping reactions at the LiPON/Cu interface were carried out at room temperature by assembling the Cu-cell in the three-electrode electrochemical cell as schematically shown in Fig. 1(a). The working electrode was the Cu film, and both the reference and counter electrodes were lithium metal. The Cu-cell was mounted at the bottom of the cell, where liquid electrolyte of 1 mol dm^{-3} $LiClO_4$/PC was immersed only at the LATP sheet bare side of the Cu-cell. The opposite side of the Cu-cell (Cu film side) was placed on stainless steel base used for the current collector. The Cu-cell was bonded in the electrochemical cell using O-ring by screws to prevent the liquid electrolyte spill. Both the LATP sheet and the LiPON film are dense lithium-ion conductive solid electrolytes, thus only the lithium ions pass through the Cu-cell and the lithium plating reaction takes place at the LiPON/Cu interface. Fig. 1(b) shows the SEM image after an initial lithium plating reaction. It should be noted that the lithium grows toward the Cu film side from the LiPON/Cu interface, which is opposite behavior to the conventional liquid electrolyte system, that is, lithium growth toward the electrolyte side from the liquid electrolyte/current collector interface. This unique plating situation resembles with the cathodic silver plating on solid electrolyte [16,17] and is good agreement with the previous report [7]. The lithium plating reaction was carried out at 5–500 μA cm^{-2} for a given time so that total plating amount becomes same value. The resultant lithium-plated samples were observed by scanning electron microscopy (SEM) without exposing the samples to the air and then the samples were observed again by *ex-situ* optical microscopy. A.C. impedance analyses (VMP 3, BioLogic) were conducted before and after the lithium plating reactions by applying a sine wave of 5 mV (rms) amplitude over the frequency range of 200 kHz to 100 mHz.

The above lithium plating process was observed through quartz glass window from the Cu film side in the Cu-cell by *in-situ* optical microscopy using three-electrode electrochemical cell schematically shown in Fig. 2. Geometry of the working, counter, and reference electrodes is same with Fig. 1 except for using Ni current collector sheet (thickness: 200 μm) with $\phi = 3$ mm hole in the center under the Cu film for the observation. As a consequence, the observed lithium plating reaction in this electrochemical cell proceeds with no pressure because the above Ni sheet was thicker than the thickness of the plated lithium.

To evaluate the advantage of morphology-controlled lithium, two kinds of half cells of LATP sheet/LiPON/Li were prepared, where Li was vacuum-evaporated lithium thin-film (V-Li) with thickness of 4–5 μm or electrochemically-grown Li plated at 500 μA cm^{-2} up to 5 μm in theoretical thickness (E-Li). Overpotential of these two cells during lithium plating reactions at 50 μA cm^{-2} was investigated. Also, different amount of lithium was sequentially plated and stripped from thin to thick state in these two cells at 3.2 mA cm^{-2} for 50 cycles where the amount was 0.13, 0.25, 0.51, and 1.0 μm in thickness.

3. Results and discussions

3.1. In-situ optical microscopy observation

Fig. 3 shows a potential profile during the lithium plating reaction at 50 μA cm^{-2} in an *in-situ* optical microscopy observation cell. Potential spike was observed at the early lithium plating process, later, the potential was gradually increased with the lithium plating reaction, and finally, the potential became almost stable value at −0.035 V (vs. Li/Li^+). Fig. 4 summarizes the *in-situ* optical microscopy images of the Cu-cell from the Cu film side during the lithium plating process shown in Fig. 3 (open circle points). Initial sample shows flat texture (Fig. 4(a)). The morphology change was slightly observed just after the potential spike (Fig. 4(b)), later, the precipitated product grew in-plane direction (Figs. 4(c)–(e)) but new products were not observed. After the potential was almost stabilized, the precipitated product grew not in-plane direction but perpendicular direction to the surface of the Cu-cell. Defocusing of the optical microscopy images during this lithium plating region (after the point f (500 s)) may be ascribed to this three-dimensional growth process. From these *in-situ* observations, it is clear that initial lithium plating morphology is largely influenced on the later lithium plating morphology because the subsequent lithium plating reaction tends to proceed preferentially at the pre-plated region. Variation of potential profiles with morphology change looks to resemble with silver plating reaction on solid electrolyte [17]. Fig. 5 shows the SEM image after a small amount of lithium plating reaction. Although lithium can diffuse inside the Cu film [7,21], the precipitated lithium grew not on the Cu film but burst through the Cu film as shown in Fig. 5, and the Cu film was lifted up and broken away from the LiPON by the lithium growth. Thus, morphology changes shown in Fig. 4(b)–(h) are reflected on the lithium plating reaction at the LiPON/Cu interface. This lifting-up phenomenon of

Fig. 5. A magnified SEM image after small amount of Li plating reaction of the LATP sheet/LiPON/Cu cell.

current corrector film during the lithium plating process has been observed also in the past work [7].

3.2. Effects of current densities on lithium plating morphology

Fig. 6 shows both the optical microscopy images and SEM ones of the Cu-cell after the initial lithium plating reactions at different current densities. The lithium plating amount was the same in any cases (18 mC, theoretical thickness: 0.13 μm). Although precipitated lithium formed a needle shape in spots at 5 μA cm^{-2}, the increasing of the current densities brought about both the increasing of the coverage ratio by precipitated lithium and the decreasing of the precipitated lithium size. The morphology change was too small to be observed at 500 μA cm^{-2}. Fig. 7(a) shows the potential change during these lithium plating reactions. The behavior of potential change resembled with Fig. 3 in any cases, but both the potential spike at the early lithium plating process and the overpotential (η_{EL}) after the lithium plating for 18 mC depended on the current densities. Fig. 7(b) shows the potential change during the lithium plating reaction to the LATP sheet/LiPON/V-Li cell. It is clear that the

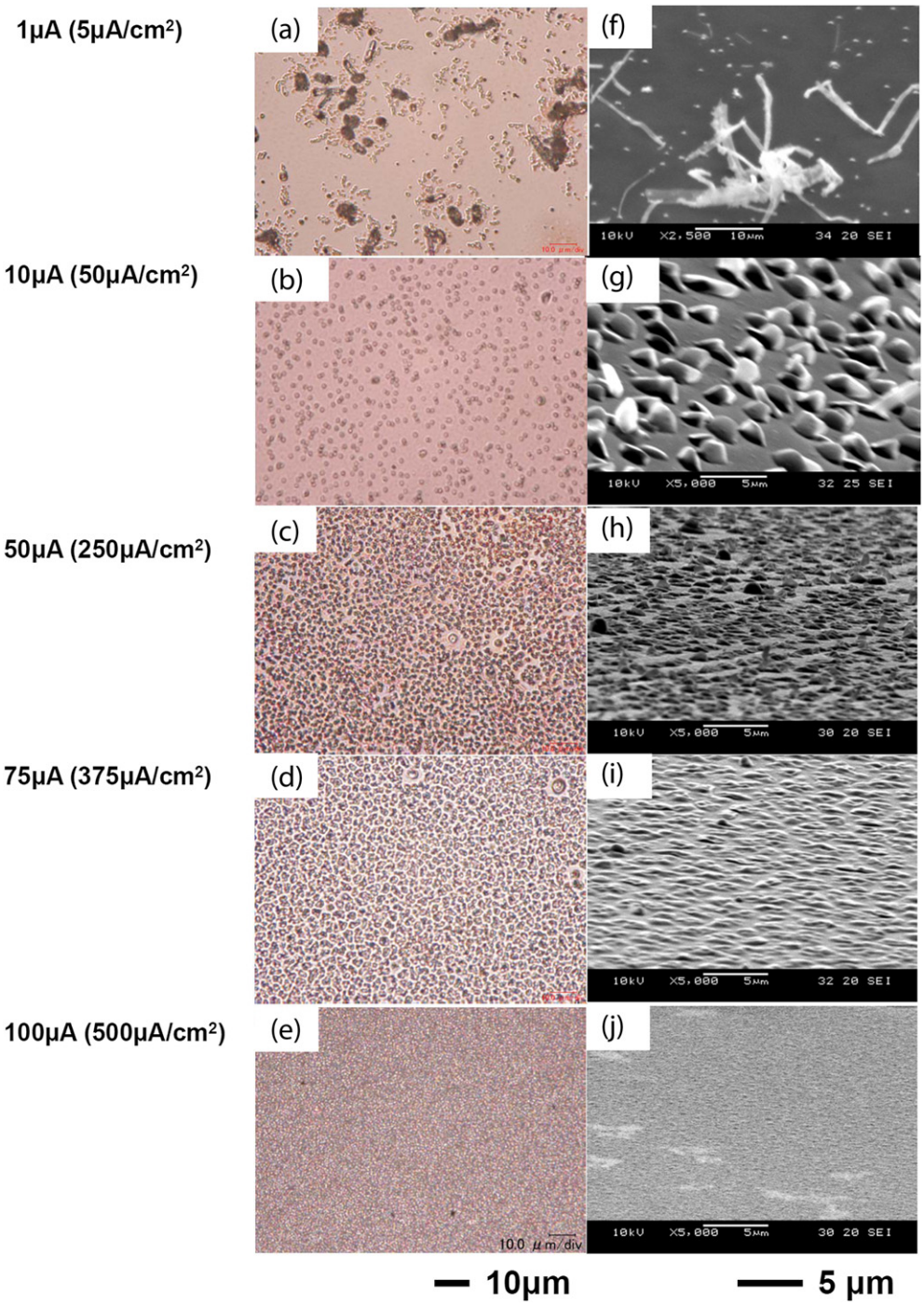

Fig. 6. Optical microscopy ((a)–(e)) and SEM images ((f)–(j)) of the LATP sheet/LiPON/Cu cell after Li plating reactions at different current densities; (a) and (f) 5, (b) and (g) 50, (c) and (h) 250, (d) and (i) 375, and (e) and (j) 500 μA cm^{-2}. Theoretical Li plating thickness was 0.13 μm in any cases.

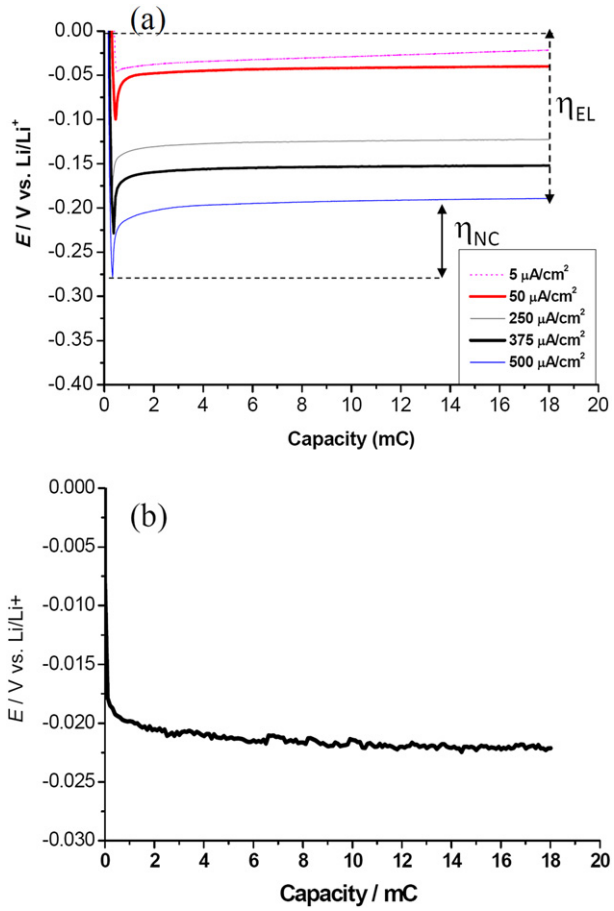

Fig. 7. (a) Initial Li plating curve of the LATP sheet/LiPON/Cu cell at different current densities. $I = 5$ (red: thin dotted line), 50 (red: thin line), 250 (gray: normal line), 375 (black: dotted bold line), and 500 (blue: bold line) μA cm^{-2}. (b) Lithium plating curve of the LATP sheet/LiPON/Li film. $I = 50$ μA cm^{-2}. (For interpretation of the references to color in this figure legend, the reader is referred to the web version of this article.)

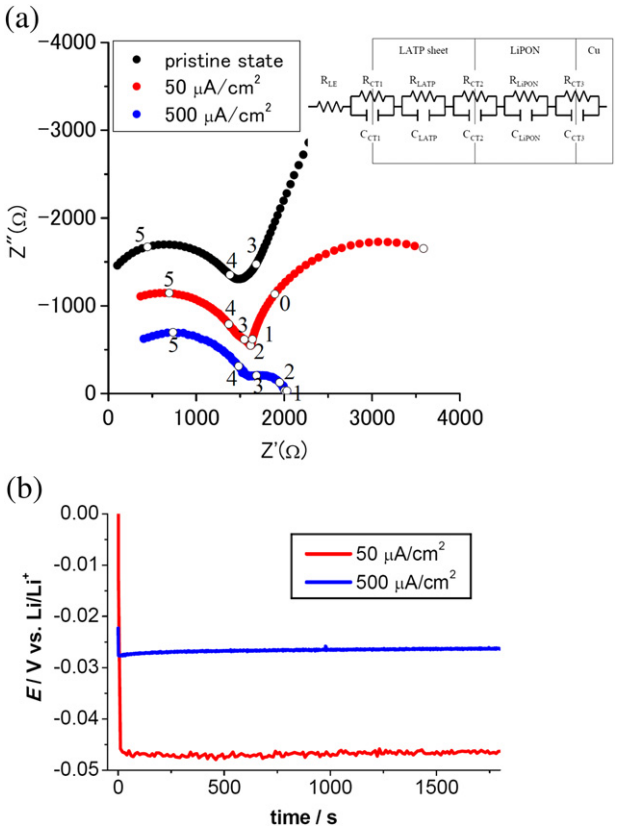

Fig. 8. (a) Cole–Cole plots of LATP sheet/LiPON/Cu cell measured in the electrochemical cell shown in Fig. 1 at pristine state (black) and after lithium plating reaction at 50 μA cm^{-2} (red) and 500 μA cm^{-2} (blue). Theoretical Li plating amount was 0.13 μm in both cases. The inset shows equivalent circuit model; R_{LE}, R_{CT1}(C_{CT1}), R_{LATP}(C_{LATP}), R_{CT2}(C_{CT2}), R_{LiPON}(C_{LiPON}), and R_{CT3}(C_{CT3}): resistance (capacitance) of liquid electrolyte, Li^+ transfer at the liquid electrolyte/LATP sheet interface, LATP sheet, Li^+ transfer at the LATP sheet/LiPON interface, and charge transfer resistance at the LiPON/current collector interface, respectively. (b) Lithium plating curve of the LATP sheet/LiPON/Cu cell at 50 μA cm^{-2} after Li plating reaction at 50 μA cm^{-2} (red: thin line) and 500 μA cm^{-2} (blue: bold line). (For interpretation of the references to color in this figure legend, the reader is referred to the web version of this article.)

initial potential spike was not observed at all in this case while the η_{EL} was recognized in the same manner. Therefore, potential spike at the early lithium plating process is influenced on the early lithium plating reaction at the LiPON/Cu film interface, most probably, nucleation and growth process.

As expected from both the *in-situ* optical microscopy observations and its potential profile, nucleation process looks to require large activation energy and then this process can be the rate determining step of the initial lithium plating reaction at the LiPON/Cu interface. At that case, charge transfer reaction of the lithium plating reaction will maintain equilibrium state, and then the electrode potential will vary with the increasing of the activity of adsorbed ad-atom as follows,

$$E^* = E_0 + \frac{RT}{F} \ln \frac{a_{LiPON}^{Li^+}}{a_{ad}}, \quad (1)$$

Table 1
Overpotential during the lithium plating reaction.

Current densities [μA cm^{-2}]	Overpotential (η_{NC}) [mV]
5	4
50	48
250	58
375	65
500	70

where E_0 is the equilibrium potential, E^* is the potential during the plating process, a_{ad} is the activity of adsorbed ad-atom (M_{ad}) at the polarized -state, $a_{LiPON}^{Li^+}$ is the activity of Li^+ in the LiPON film, R is gas constant, T is absolute temperature, and F is Faraday constant. Also, Nernst equation for the lithium plating reaction is

$$E = E_0 + \frac{RT}{F} \ln \frac{a_{LiPON}^{Li^+}}{a_{ad}^{\circ}}, \quad (2)$$

where E is the electrode potential, a_{ad}° is activity of M_{ad} under the equilibrium state. Here, the difference between the E^* and the E is the overpotential for the crystallization process ($\eta_K = E^* - E$) [22]. The increasing of the current densities will increase the activity of M_{ad} as follows,

$$a_{ad} = a_{ad}^{\circ} \exp\left(\frac{F\eta_K}{RT}\right) \quad (3)$$

The η_K is proportional to the change of chemical potential ($\Delta\mu$) for the incorporation of ad-atom into an embryo as follows,

$$\Delta\mu = F\eta_K \quad (4)$$

The increasing of $\Delta\mu$ in turn decreases both the critical radius (r_C) of nuclei and the activation energy for the nucleation reaction ($\Delta G^{\#}$) according to the below equations

$$r_C = \frac{\gamma V}{\Delta\mu} \tag{5}$$

$$\Delta G^{\#} = \frac{\pi h \gamma^2}{F\eta_K}, \tag{6}$$

where V is atomic volume, γ is Gibbs energy per unit length along the embryo, h is height of disk-shaped embryo. In equation (6), the $\Delta G^{\#}$ is estimated by assuming the formation of disk-shaped embryo. These equations mean that the increasing of the η_K decreases both the critical radius and the activation energy for the nucleation, resulting in the smaller-sized precipitation. Table 1 summarizes the values of the potential spike (η_{NC}) which were estimated just by subtracting the maximum overpotential at each potential spike from the η_{EL}. Although precise value of the η_K cannot be estimated from Fig. 7(a), variation of the η_{NC} was consistent with the expected trend of those of η_K from equation (6). The critical size of nuclei is generally much less than micron order, thus the precipitations with micron order in Fig. 6 may be grown by the coalescence of the nuclei.

A.C. impedance analyses were carried out at open circuit voltage after the lithium plating reactions at 50 or 500 μA cm^{-2}. As shown in Fig. 8(a), the spectrum measured before lithium plating reaction consisted of one semicircular arc at high frequency region, followed by a straight line to the real axis. The inset shows the equivalent circuit model expected from the electrochemical measurement cell shown in Fig. 1. Based on this model, potential-independent semicircular arc must be mixture of various components, that is, electrolyte resistances (liquid electrolyte (R_{LE}), LATP sheet (R_{LATP}), and LiPON film (R_{LiPON})) and interfacial Li^+-transfer resistances (liquid electrolyte/LATP interface (R_{CT1}) and LATP/LiPON (R_{CT2})). After the lithium plating reactions, semicircular arc was newly appeared at low frequency region in both samples, and the diameter of the lithium-plated sample by 500 μA cm^{-2} was much smaller than that by the 50 μA cm^{-2}. This newly appeared semicircular arc will be assigned to the charge transfer resistance at the LiPON/current collector interface (R_{CT3}) because only this reaction is considerable potential-dependent semicircular arc. As shown in Fig. 4, lithium tends to grow from the lithium pre-plated region probably because lithium requires extra-large energy to create new plating sites as discussed in the previous section. Thus, lithium pre-plated region will mainly work as charge transfer sites. Fig. 8(b) shows the lithium plating curves at 50 μA cm^{-2} to the samples with lithium pre-plated at 50 or 500 μA cm^{-2}. In both cases, potential spike was not almost observed at the early lithium plating process. It is clear that the sample with lithium pre-plated at 500 μA cm^{-2} shows smaller overpotential than that of the 50 μA cm^{-2}. This is because smaller charge transfer resistance is achieved to the sample plated at 500 μA cm^{-2} by larger number of charge transfer sites due to smaller-sized precipitations of lithium as shown in Fig. 6(e) and (j). These results indicate that regulation of the lithium plating morphology is effective to reduce the charge transfer resistance at the LiPON/current collector interface.

3.3. Application of the in-situ electrochemical lithium growth regulation

Fig. 9(a) and (b) shows the surface SEM images of the V-Li and E-Li, respectively. The surface texture of the V-Li was flat, while that of the E-Li was rough. Fig. 9(c) shows the potential profile of

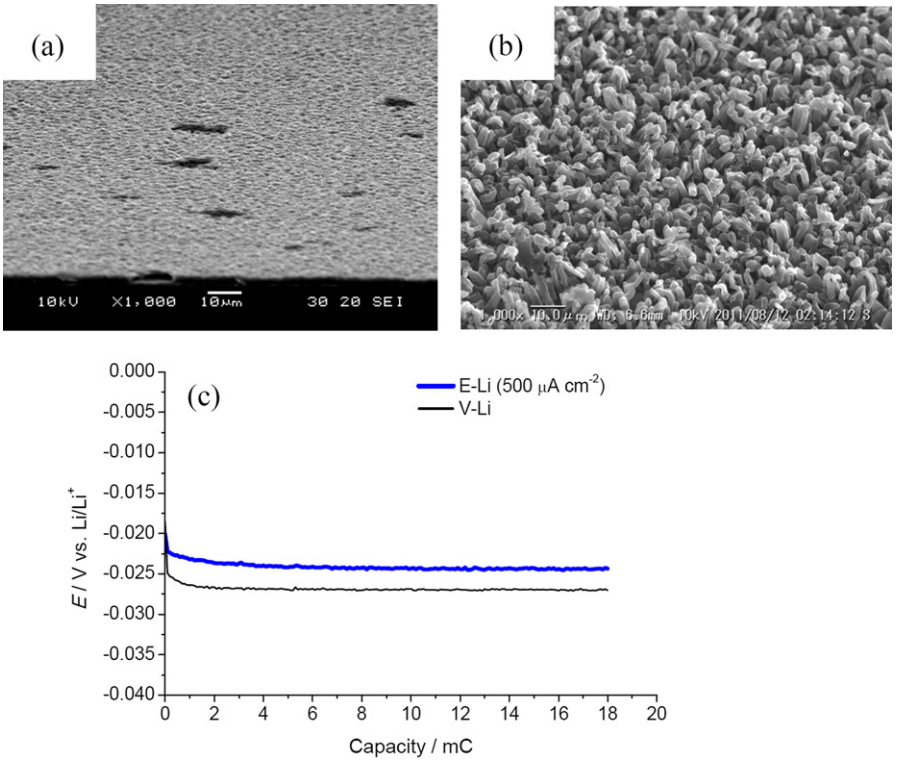

Fig. 9. SEM images of (a) the vacuum-evaporated Li film (thickness: 5 μm) and (b) electrochemically-grown Li at 500 μA cm^{-2} with theoretical plating thickness of 5 μm. (c) Lithium plating curve at 50 μA cm^{-2} of the LATP sheet/LiPON/vacuum-evaporated Li film (black: thin line) and the LATP sheet/LiPON/electrochemically-grown Li film (blue: bold line). (For interpretation of the references to color in this figure legend, the reader is referred to the web version of this article.)

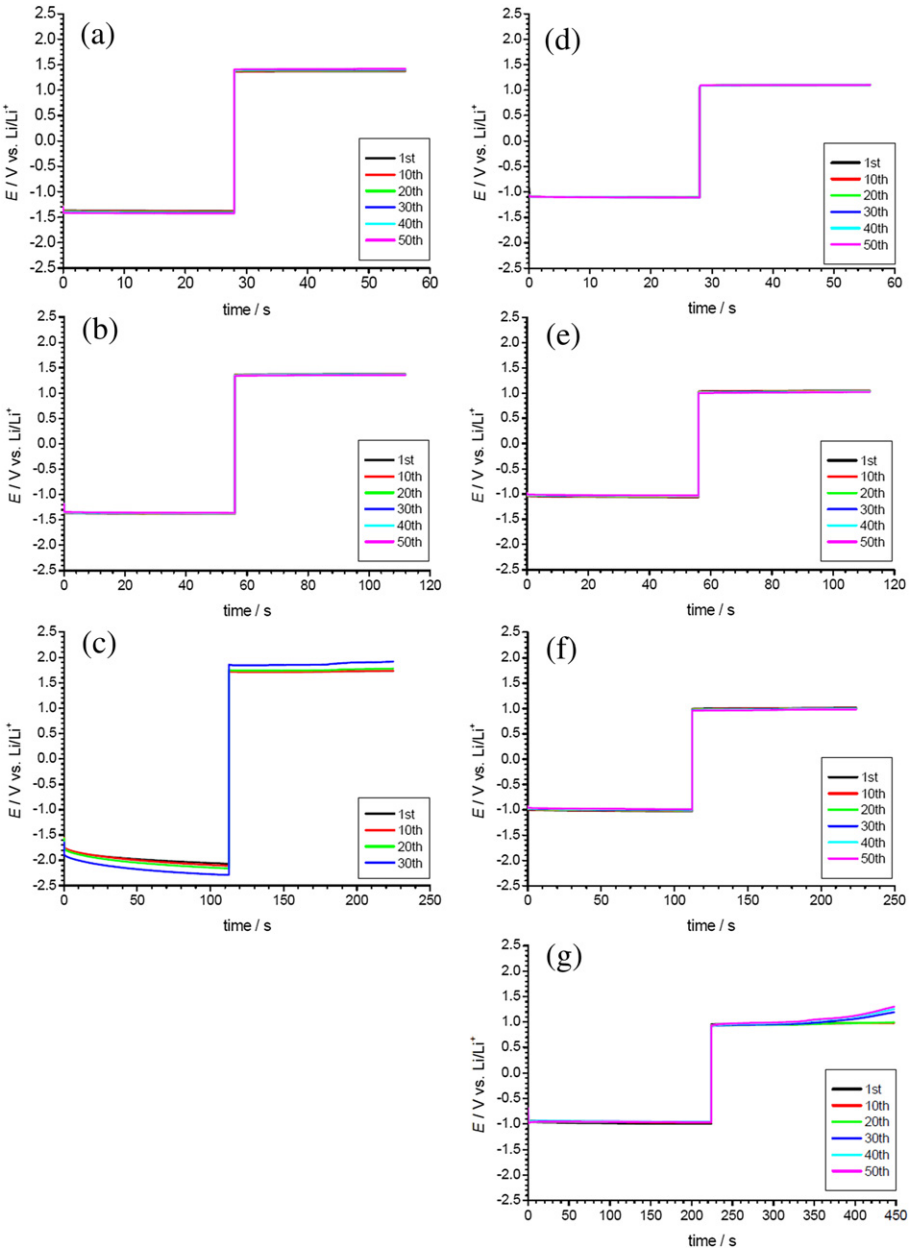

Fig. 10. Lithium plating-stripping curves at 3.2 mA cm^{-2} for 50 or 30 times of (a)–(c) LATP sheet/LiPON/vacuum-evaporated Li cell (V-Li-cell) and (d)-(g) LATP sheet/LiPON/electrochemically-grown Li cell (E-Li-cell). The plating-stripping amount was (a) (d) 0.13 μm, (b) (e) 0.25 μm, (c) (f) 0.51 μm, and (g) 1.0 μm. Those reactions were sequentially carried out from thin to thick state after 50 times plating-stripping reactions at each plating amount.

the lithium plating reaction at 50 μA cm^{-2} to these cells. The E-Li has slightly smaller overvoltage than that of the V-Li, probably because the electrochemically grown lithium provides well-connected and uniform interface with LiPON film as compared with the V-Li.

Fig. 10 summarizes the lithium plating-stripping reaction curves at 3.2 mA cm^{-2} of both the LATP sheet/LiPON/V-Li cell (V-Li-cell) and the LATP sheet/LiPON/E-Li cell (E-Li-cell). The V-Li-cell repeated the plating-stripping reactions maintaining the overpotential of ca. 1.3 V by the plating-stripping amount of 0.25 μm in thickness (Fig. 10(a) and (b)). However, when the amount was increased up to 0.51 μm, larger overpotential was observed at the lithium plating reaction. On the other hand, the E-Li-cell repeated reactions maintaining overpotential of ca. 1.0 V for 50 cycles by the thickness of 0.51 μm. This overpotential was maintained even at the lithium plating-stripping amount of 1 μm in thickness for several cycles, but in later cycles, the overpotential gradually increased during the stripping process. Because this undesirable increasing of the overpotential was suppressed by pressing the electrochemical cell with appropriate value during the reactions, formation of cavity around the interface may degrade the reaction. Details of this phenomenon are currently investigated.

4. Conclusion

Effects of current densities on the lithium plating morphology between a lithium phosphorus oxynitride glass electrolyte (LiPON)/copper (Cu) thin film was investigated. The increasing of the current density decreased the size of plated lithium probably because of the increasing of the crystallization overpotential. *In-situ* optical

microscopy observations showed that lithium tends to grow at the lithium pre-plated region. Thus, the regulation of the initial lithium plating morphology is an important factor to stabilize the subsequent lithium plating-stripping reactions and reduce its charge-transfer resistance.

The electrochemically-grown lithium plated at 500 μA cm^{-2} showed stable and lower resistive lithium plating-stripping reactions even against the vacuum-evaporated lithium. Electrochemical growth will develop low- and uniform-resistive interface, which reduces inhomogeneous lithium plating-stripping reactions and then stabilize the reactions. However, this stability was not maintained when thicker lithium was plated-stripped (1 μm in thickness) for several cycles. Because this unstability was improved by pressing the sample with appropriate pressure, formation of cavity around the interface may degrade the reaction.

Acknowledgment

The authors would like to express great appreciation to Mr. Hirofumi Yamamoto for technical supports of SEM observations. This work was financially supported by JST-CREST, and also partially by JST-ALCA.

References

[1] J.M. Tarascon, M. Armand, Nature 414 (2001) 359.
[2] J.B. Bates, N.J. Dudney, G.R. Gruzalski, R.A. Zuhr, A. Choudhury, C.F. Luck, J.D. Robertson, Solid State Ionics 53-6 (1992) 647.
[3] B. Wang, J.B. Bates, F.X. Hart, B.C. Sales, R.A. Zuhr, J.D. Robertson, J. Electrochem. Soc. 143 (1996) 3203.
[4] E.J. Jeon, Y.W. Shin, S.C. Nam, W.I. Cho, Y.S. Yoon, J. Electrochem. Soc. 148 (2001) A318.
[5] S.H. Lee, P. Liu, C.E. Tracy, Electrochem. Solid State Lett. 6 (2003) A275.
[6] Y. Iriyama, K. Nishimoto, C. Yada, T. Abe, Z. Ogumi, K. Kikuchi, J. Electrochem. Soc. 153 (2006) A821.
[7] B.J. Neudecker, N.J. Dudney, J.B. Bates, J. Electrochem. Soc. 147 (2) (2000) 517.
[8] B. Fleutot, B. Pecquenard, F. Le Cras, B. Delis, H. Martinez, L. Dupont, D. Guy-Bouyssou, J. Power Sources 196 (2011) 10289.
[9] K. Okita, K. Ikeda, H. Sano, Y. Iriyama, H. Sakaebe, J. Power Sources 196 (2011) 2135.
[10] T. Takahashi, O. Yamamoto, Electrochim. Acta 11 (1966) 911.
[11] N. Kimura, T. Osaki, S. Toshima, Bull. Chem. Soc. Jpn. 48 (1975) 830.
[12] R. Waser, R. Dittmann, G. Staikov, K. Szot, Adv. Mater. 21 (2009) 2632.
[13] A. Spangenberg, J. Fleig, J. Maier, Adv. Mater. 13 (2001) 1466.
[14] T. Takahashi, O. Yamamoto, Denkikagaku 32 (1964) 664.
[15] Y.-G. Guo, Y.-S. Hu, J.-S. Lee, J. Maier, Electrochem. Commun. 8 (2006) 1179.
[16] J. Corish, C.D. O'Briain, J. Mater. Sci. 6 (1971) 252.
[17] T. Ohachi, I. Taniguchi, J. Cryst. Growth 24/25 (1974) 362.
[18] K. Peppler, J. Janek, Solid State Ionics 177 (2006) 1643.
[19] K. Peppler, J. Janek, Electrochim. Acta 53 (2007) 319.
[20] http://www.ohara-inc.co.jp/en/product/electronics/licgc.html.
[21] J. Suzuki, K. Sekine, T. Takamura, Electrochemistry 71 (2003) 1120.
[22] K.J. Vetter (Ed.), Electrochemical Kinetics – Theoretical and Experimental Aspects, Academic Press Inc., London, 1967.